Lab on a Chip

Micro- & nano- fluidic research for chemistry, physics, biology, & bioengineering

www.rsc.org/loc

Volume 10 | Number 5 | 7 March 2010 | Pages 529–668

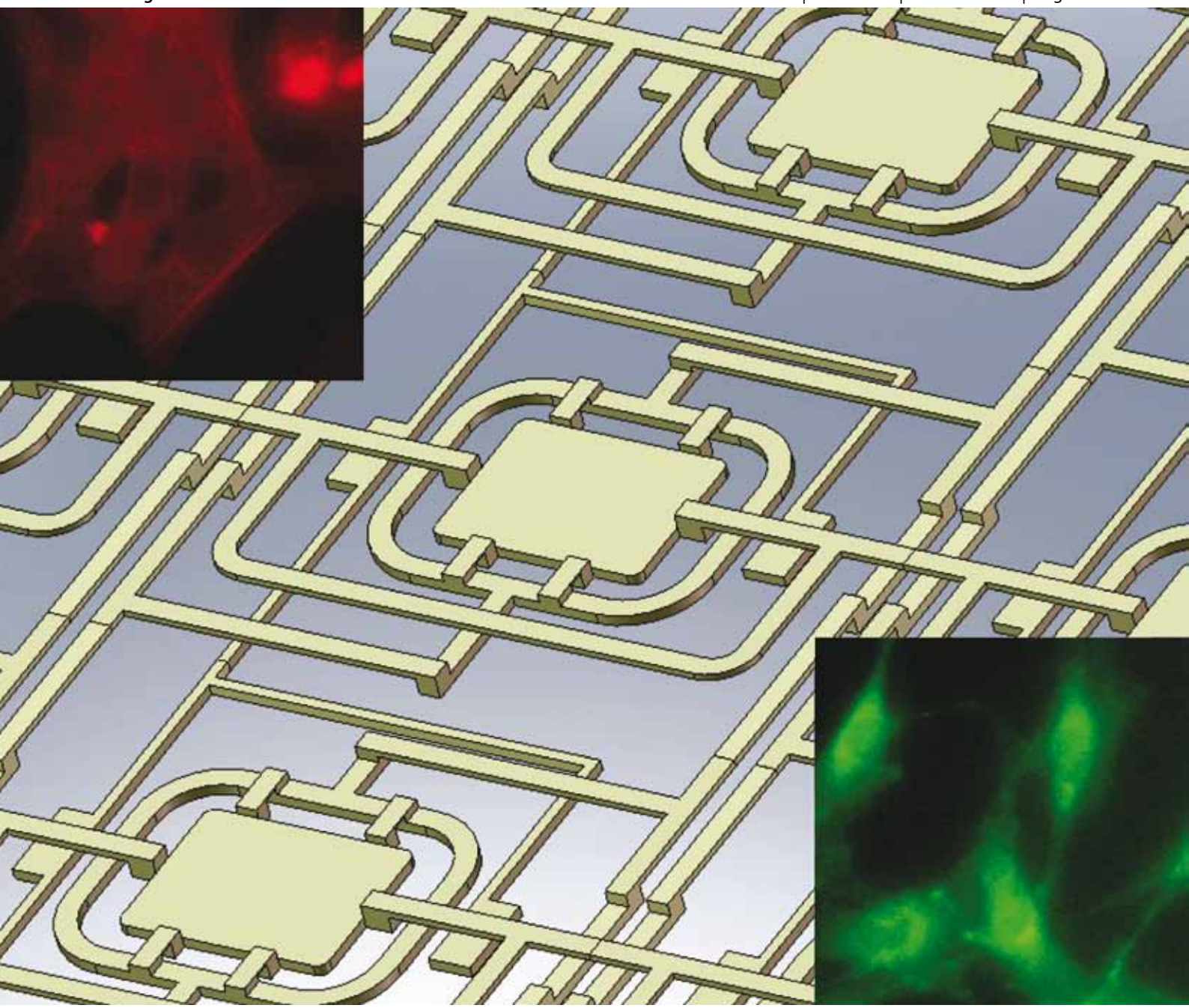

ISSN 1473-0197

RSC Publishing

Continuously perfused, non-cross-contaminating microfluidic chamber array for studying cellular responses to orthogonal combinations of matrix and soluble signals†

Edward S. Park,[a] Ashley C. Brown,[b] Michael A. DiFeo,[a] Thomas H. Barker[bcd] and Hang Lu*[acd]

Received 16th September 2009, Accepted 25th November 2009
First published as an Advance Article on the web 23rd December 2009
DOI: 10.1039/b919294h

We present a microfluidic cell culture array with unique versatility and parallelization for experimental trials requiring perfusion cultures. Specifically, we realize a rectangular chamber array in a PDMS device with three attributes: (i) continuous perfusion; (ii) flow paths that forbid cross-chamber contamination; and (iii) chamber shielding from direct perfusion to minimize shear-induced cell behaviour. These attributes are made possible by a bridge-and-underpass architecture, where flow streams travel vertically to pass over (or under) channels and on-chip valves. The array is also designed for considerable versatility, providing subarray, row, column, or single chamber addressing. It allows for incubation with adsorbed molecules, perfusion of differing media, seeding or extraction of cells, and assay staining. We use the device to characterize different phenotypes of alveolar epithelial type II (ATII) cells, particularly the extent of epithelial-to-mesenchymal transition (EMT), a highly suspected pathway in tissue regeneration and fibrosis. Cells are cultured on combinations of matrix proteins (fibronectin or laminin by row) and soluble signals (with or without transforming growth factor-β1 by column) with two repeats per chip. Fluorescent assays are performed in the array to assess viability, cytoskeletal organization, and cell–cell junction formation. Assay and morphological data are used to tease-out effects of cues driving each phenotype, confirming this as an effective and versatile combinatorial screening platform.

Introduction

Over the past several years, numerous works have demonstrated the utility of microfluidic arrays as screening tools to culture cells in diverse microenvironments.[1–6] Interest in microfluidic systems arises from the prospect of very low sample usage, highly-parallelized experiments, and well-controlled culture conditions, all of which are facilitated through miniaturization. With respect to microenvironments, the screening of cellular responses to simultaneous stimulation of soluble and extracellular matrix (ECM) cues is a broad line of inquiry that is particularly useful in studying phenotype transitions. Epithelial-to-mesenchymal transition (EMT) is one such transition that is implicated in numerous developmental and pathological processes. Greater understanding of phenotype transitions could lead to new therapeutic approaches, facilitated by microfluidic arrays with new capabilities.

[a]*School of Chemical & Biomolecular Engineering, Georgia Institute of Technology, Atlanta, GA, USA. E-mail: hang.lu@chbe.gatech.edu; Fax: +404 894 4200; Tel: +404 894 8473*
[b]*Department of Biomedical Engineering, Georgia Institute of Technology and Emory University, Atlanta, GA, USA*
[c]*The Parker H. Petit Institute of Bioengineering and Biosciences, Georgia Institute of Technology and Emory University, Atlanta, GA, USA*
[d]*Interdisciplinary Program of Bioengineering, Georgia Institute of Technology and Emory University, Atlanta, GA, USA*
† Electronic supplementary information (ESI) available: PDF with additional commentary on device design, fabrication, and experimentation, as well as 6 figures and an AVI movie of cell loading. See DOI: 10.1039/b919294h

Microfluidic chamber arrays have been developed in many forms, and most can be categorized into one of three generalized architectures. First, there are open array architectures, where all chambers are fluidically linked, allowing flow and diffusional transport among chambers.[7–11] The extent of cross-chamber communication (convective or diffusional) is determined by the flow rate, flow direction, and device geometry. Second, there are architectures isolated by rows/columns, where flow is restricted to individual rows (or columns) by valves or other barriers.[12–16] Therefore, only communication among chambers within rows (or columns) is possible. Signals secreted from cells in upstream chambers may be a concern, the extent of which depends upon the signal and its concentration, which in turn is determined by cell density, secretion rate, and flow velocity. Third, there are architectures where the chambers are completely isolated from each other and individually addressed. This eliminates cross-chamber communication by extensive use of on-chip valves and bussing channels.[17,18]

In addition to the general array architecture, the chamber design is also an important feature, particularly with respect to shear stress.[19] Undesired shear-induced cell behaviour can be minimized by the use of flow barriers to protect cells from shear[8] or by recessing the chamber from the main flow path.[7,14]

In this work, we introduce a microfluidic array architecture that demonstrates a novel combination of attributes: continuous-perfusion through each chamber, no cross-chamber communication (*i.e.* contamination), and chamber shielding to reduce shear stresses experienced by cells. At the same time, a high degree of versatility is offered, as well as experimental parallelization.

We demonstrate the utility of this device by studying the effect of extracellular matrix (ECM) proteins fibronectin (Fn) and laminin (Ln), in conjunction with the soluble transforming growth factor- β1 (TGF-β1), on the extent of EMT in alveolar epithelial cells. This requires a combinatorial experimental setup that takes advantage of the attributes of our device design. While the experiments conducted here are meant as a validation of previous findings regarding the role of ECM in the regulation of epithelial cell responses to TGF-β1, understanding the complex integration of extracellular signals on cell fate has significance in the study of tissue development, homeostasis, repair/regeneration, and pathology. Enabling massively parallel interrogation of orthogonal substrate and soluble signals will contribute significantly to the rapid identification of critical integrin-growth factor receptor synergistic signals regulating complex cell behaviours, as well as the ability to rapidly screen potential therapeutic compounds to regulate such complex cellular behaviours.

Experimental

Fabrication

A schematic of the device architecture is shown in Fig. 1, highlighting the main attributes and features (chamber and channels) associated with a unit cell of the array. Devices are fabricated using a combination of techniques, including soft lithography,[20] multi-layer PDMS thermal bonding,[21] and through-hole processing. Fabrication requires two master molds (masters A and B). Each master is a silicon wafer (100 mm diameter) with a photoresist pattern forming device features in positive relief. Photoresist patterns are realized using standard photolithographic methods.[22]

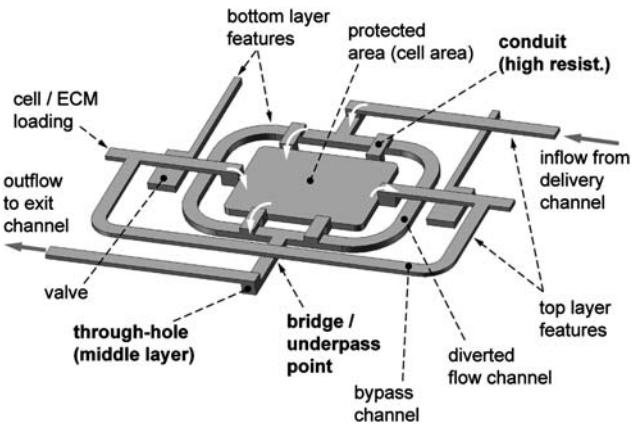

Fig. 1 Schematic of device architecture. Three-dimensional flow network requires through-holes (middle layer) that fluidically connect top and bottom layers. White arrows indicate selected locations where flow travels 3-dimensionally. (i) Chamber is continuously-perfused by inflowing medium. (ii) Cross-chamber communication is avoided; fresh medium from a delivery channel (not shown) flows through the chamber and into an exit channel (also not shown). (iii) High-resistance conduits on chamber ceiling shield the protected area from the majority of flow. The chamber, along with supporting channel network, is repeated to realize a 2 × 4 prototype array device. Three-dimensional flows and bridge/underpass points are essential to implement a rectangular array of chambers with continuous perfusion, no cross-chamber communication, and versatility described in this work.

Master A contains a two-layer pattern of SU-8 (MicroChem Corp., Newton, MA, USA), a negative-type photoresist. The first layer is 50 μm tall, and its features define the "bottom" device layer. The second layer, which is patterned on the first layer, is 30 μm tall with features defining the "middle" device layer (*i.e.* through-holes).

Master B contains patterns made of both AZ P4620 (AZ Electronic Materials Corp., Branchburg, NJ, USA), a positive-type photoresist, and SU-8. The AZ P4620 features (35 μm tall) define flow channels. These channels have a semi-circular cross-section, allowing them to be fully closed by push-up valves located throughout the device. The SU-8 features (7 μm tall) correspond to conduits (four for each chamber) that allow perfusion through the chamber ceilings (Fig. 1). See ESI for further discussion of master mold fabrication.†

Devices are made of poly(dimethylsiloxane) (PDMS) using the process summarized in Fig. 2(a). Through-holes are realized by adapting the compression-molding techniques of Folch *et al.*[23] and Kim *et al.*[24] with certain modifications. Briefly, PDMS (Sylgard 184, Dow Corning Corp., Midland, MI, USA) with a base-to-curing agent ratio of 20 : 1 is mixed and degassed under vacuum in a desiccator for 2 h. The PDMS is then spin coated onto master A to a thickness of 200 μm. A mylar transparency is laminated on top of the PDMS; care is taken not to introduce bubbles between the transparency and PDMS. More transparencies are added, including small device-sized transparencies located above device positions (see ESI Fig. 1†). Additionally, a blank silicon wafer, cloth sheets (TechniCloth II, ITW Texwipe, Mahwah, NJ, USA), and steel blocks (total weight ~40 lbs) are placed on the stack to displace PDMS from the top of the tallest SU-8 features. The entire stacked assembly is placed on a flat bake plate (CEE 100CB plate, Brewer Science Inc., Rolla, MO, USA) at 80 °C for 10.5 min. After cooling, the stack is disassembled, and the transparency is peeled off the PDMS surface. Hence, master A is left with a layer of partially cured PDMS that is the same height as the tallest SU-8 features (~80 μm); the tops of such features are devoid of residual PDMS, resulting in well-defined through-holes.

The PDMS on master A is aligned and bonded to a subsequent PDMS layer, which is derived from master B as follows. PDMS with a base-to-curing agent ratio of 5 : 1 is mixed, degassed (2 h), and poured onto master B to a thickness of 4 mm. The PDMS is cured at 70 °C in a convection oven for 20 min. After cooling, the PDMS is peeled off the master and cut into individual device slabs. Inlet and outlet ports are cored through the slabs using 20G luer stubs.

Each slab is aligned and attached to corresponding locations on the PDMS layer of master A. The two layers are then cured at 70 °C for at least 4 h to fully bond into a monolithic device. After cooling, the devices are peeled off the master, and valve control ports are cored through the devices using 21G luer stubs. Finally, each device, along with a glass slide, is exposed to air plasma for 30 s (Plasma Cleaner PDC-32G, Harrick Plasma, Ithaca, NY, USA), and the two are brought into contact and irreversibly bonded. Thus, each microfluidic "chip" is comprised of a PDMS device containing all the topographical features (channels, chambers, through-holes, *etc.*) bonded to a glass substrate. A 2 × 4 array of cell culture chambers is in each device.

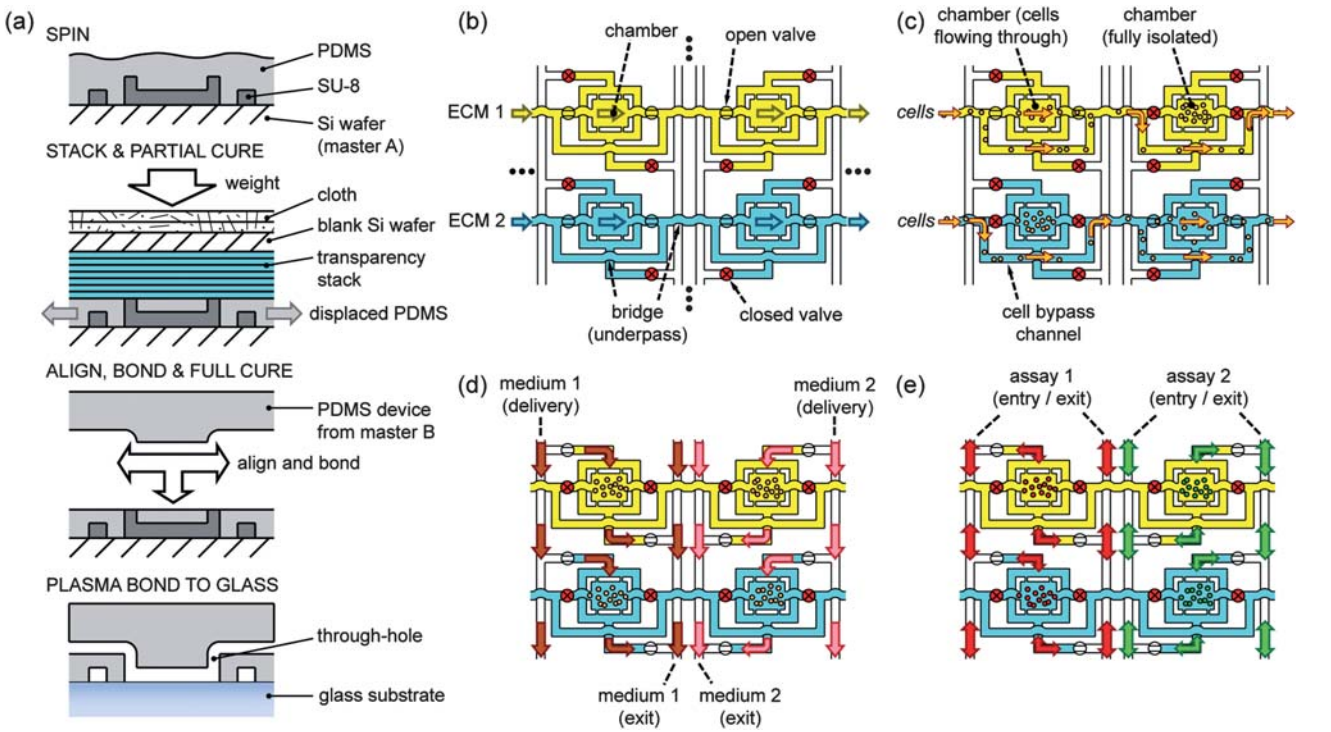

Fig. 2 Device fabrication (a) and selected modes of operation shown in a subarray of 4 chambers (b–e). (a) PDMS devices are fabricated using soft lithography, thermal bonding, and compression-molding. To improve yield of well-defined through-holes, modifications to previously reported compression-molding techniques were developed (see Results and Discussion and ESI†). (b) ECM incubation: matrix molecules adsorb to chamber surfaces by rows or individual chambers. (c) Cell loading: cell suspension flows into rows, and chambers are isolated (individually or together) to confine cells. Cells attach and spread. (d) Culture: Perfusion of different media by columns. Channel architecture directs flows over/under other flows to avoid cross-chamber communication. (e) Assay: Solutions flow through the entry or exit channels to label cells with desired probes. Illustrations not to scale.

Simulation of chamber flow field

The chamber is designed to provide continuous perfusion while protecting cells from adverse shear stress. To achieve these effects, a barrier is used to divert the majority of flow around a protected area where cells grow. Conduits (with high hydraulic resistance) on the ceiling of the chamber are intended to allow adequate mass transport through the protected area to nourish cells without undesired shear. To validate this rationale, a 3-dimensional finite element model of the chamber is constructed using the COMSOL software package (Multiphysics 3.3, COMSOL AB, Stockholm, Sweden).

The geometry of the model represents a half chamber, which exploits the two-fold symmetry of the design. All boundary conditions are no-slip, except for the inlet, outlet, and symmetry boundaries. Flow is driven by imposing a pressure drop between the inlet and outlet (positive pressure at inlet boundary and zero pressure at outlet boundary). The Navier–Stokes equations are solved at a variety of flow rates, using water as the medium. The resulting flow fields are used to generate flow velocity profiles and compare residence times through the diverted and protected areas of the chamber (Fig. 4 later).

Cell culture off-device

RLE-6TN cells (ATCC, Manassas, VA, USA), a rat-derived ATII cell line, are maintained in D-MEM/F-12 medium (Gibco 10565, Invitrogen, Carlsbad, CA, USA) with 10% fetal bovine serum and 1% penicillin/streptomyocin. Cells are incubated at 37 °C and 5% CO_2, and medium is changed every 48–72 h.

Prior to each trial, cells are detached from their culture flask using trypsin-EDTA solution (0.25% w/v trypsin and 0.53 mM EDTA, Gibco 25200, Invitrogen, Carlsbad, CA, USA). Once the cells are detached, excess medium is added, and the suspension is centrifuged. The supernatant is aspirated, and the cells are resuspended in medium to a density of $\sim 3 \times 10^6$ cells/mL and loaded into the device.

Microscope setup and supporting apparatus

Device preparation, cell loading, and assays are performed on a DM IRB/E inverted microscope (Leica Microsystems GmbH, Wetzlar, Germany) at 10× or 20× magnification in phase contrast mode or fluorescence mode (ESI Fig. 2). Hollow stainless steel pins (L-shaped, 21G) are press-fitted into device ports and are connected to flexible plastic tubing (PE-60) for fluid and pressure delivery. Perfusion is driven by syringe pump (PHD 2000, Harvard Apparatus, Holliston, MA, USA). Pressurization of on-chip valves is regulated by off-chip miniature solenoid valves (Hargraves Technology Corp., Mooresville, NC, USA) attached to a pressure source at 30 psig. Images are captured using a digital CCD camera (ORCA C4742-95-12, Hamamatsu Photonics, Hamamatsu City, Japan). Valve actuation and image capture are computer-controlled using a custom-designed interface written in the LabVIEW programming environment (National Instruments Corp., Austin, TX, USA).

Device preparation and cell culture in-device

Devices are prepared to culture cells under four different signal combinations: Fn only, Ln only, Fn with TGF-β1, and Ln with TGF-β1. Fn and Ln (33016 and 23017, respectively, Invitrogen, Carlsbad, CA, USA) solutions used for incubation are both 50 nM concentration in phosphate buffered saline (PBS). When present, TGF-β1 (R&D Systems, Minneapolis, MN, USA) concentration is 5 ng/mL.

Each device is pre-filled with PBS. To prevent on-chip valves from introducing gas bubbles into the device during experiments, each valve is filled with water. Solutions of ECM protein are introduced through row inlet ports, and each solution is addressed to selected chambers by opening the appropriate on-chip valves. The ECM is incubated at 37 °C for 1 h to allow matrix molecules to adsorb to chamber surfaces. Following ECM adsorption, the device is filled with heat-denatured BSA solution (1% w/v in PBS) and incubated at room temperature for 30 min to block surfaces from non-specific binding. The device is then flushed with additional PBS, and rows are isolated from each other with on-chip valves.

Cell suspension is then introduced into the inlet of each row and flows through all chambers in the row. Cells are confined to a chamber by closing its chamber isolation valves. Bypass channels allow cells to travel around closed chambers to other chambers. If the density or distribution of cells in a chamber is unsatisfactory, the isolation valves can be momentarily re-opened and closed to sample another set of cells.

The device is transferred from the microscope to an incubator at 37 °C and 5% CO_2. Medium is introduced into medium inlet ports and perfuses through each column at 0.3 μL/min.

Cell assays

All assays are performed after 48 h in culture in the device. Cell viability is determined by staining with two-probe LIVE/DEAD® solution (L-3224, Invitrogen, Carlsbad, CA, USA) prepared by the manufacturer's specifications (2 μM calcein AM and 4 μM ethidium homodimer-1 in PBS). LIVE/DEAD solution is introduced to the device through an assay port (ESI Fig. 3), flow is stopped, and the stain is incubated for 30 min before imaging.

To characterize differences in spreading and cell shape in response to culture conditions, actin cytoskeletons are labeled with Texas Red®-X phalloidin (T7471, Invitrogen, Carlsbad, CA, USA) and imaged. The following washes are flowed through the array: (i) fix with 4% v/v paraformaldehyde in D-MEM/F-12 medium for 15 min; (ii) PBS rinse; (iii) acetone permeabilization for 10 min; (iv) PBS rinse; and (v) phalloidin in PBS (160 nM, prepared by manufacturer's protocol) for 20 min. Flows are ~1 μL/min. Washes are performed by alternating the introduction of the different solutions through the assay/exit ports.

To characterize differences in the extent of epithelial junction formation, immunofluorescent staining for E-cadherin is performed. The following washes are flowed through the array: (i) fix with 4% v/v paraformaldehyde in D-MEM/F-12 medium for 10 min; (ii) PBS rinse; (iii) Triton X-100 (0.5% w/v in PBS) permeabilization for 10 min; (iv) PBS rinse; (v) goat serum (10% v/v in PBS) blocking for 15 min; (vi) primary antibody (36/E-Cadherin, BD Transduction Laboratories, San Jose, CA, USA) in PBS + 0.2% w/v Tween (PBST) static incubation for 12 h overnight; (vii) PBST rinse; (viii) secondary antibody in PBST (Alexa Fluor® 488-conjugated goat-anti-mouse, Santa Cruz Biotech Inc., Santa Cruz, CA, USA) static incubation for 1 h; and (ix) PBST rinse. Optimization of the protocol showed that Triton X-100 permeabilization produces better-quality fluorescent images (more visible staining) compared to acetone permeabilization. All flows are ~1 μL/min, and the introduction of different solutions is alternated between assay/exit ports.

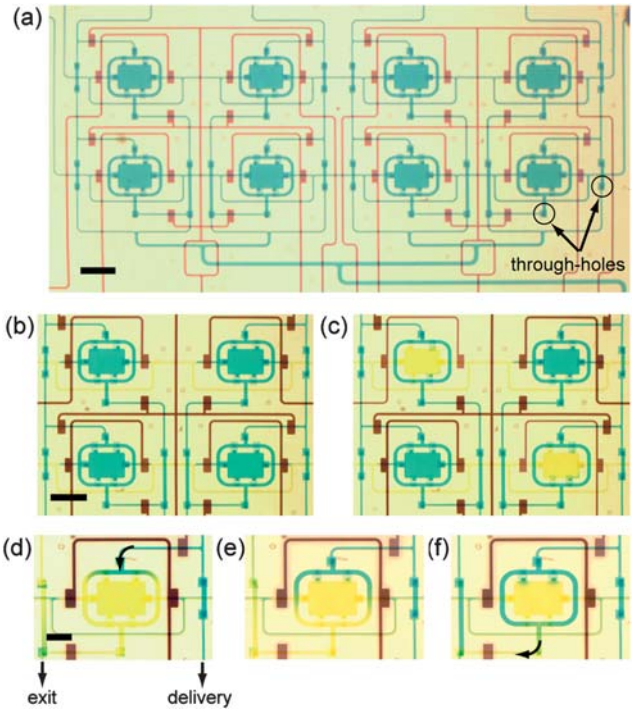

Fig. 3 Flow characterization with colored dyes. (a) Prototype device is a 2 × 4 chamber array. Blue dye loaded in 3-D flow channel/chamber network; darker square features indicate through-hole locations. Purple dye in valve control channels. (b–c) Chambers can be individually addressed with ECM, cells or assay solution. Yellow dye displaces blue dye in 2 chambers. (d–f) Cross-chamber communication avoided by routing flow through each chamber from delivery channel to exit channel (curved arrows). Upper-right valve is opened and blue dye flows through chamber. Images at 5, 10, and 20 s after valve opens at experimental flow rate. Flow into the protected area is markedly slower due to high-resistance conduits. Scale bars: (a–c) 1000 μm, (d–f) 500 μm.

Data analysis

To quantify morphological differences, cells are traced by polylines using image processing software (Image-Pro 6.1, Media Cybernetics Inc., Bethesda, MD, USA). Sample cell traces are shown in ESI Fig. 4. Circularity and area of cells is calculated for each culture condition (30 randomly selected cells per condition, 10 from each of 3 trials). Circularity, C, is defined as $C = 4\pi A/(P^2)$, where A is cell area and P is cell perimeter. A circularity of 1 corresponds to a perfectly circular shape.

For LIVE/DEAD assays, cells emitting on each fluorescent channel (green/red) are counted for each condition (6 trials per condition), and percentages live/dead are calculated.

All statistical analyses are performed by multi-variate ANOVA using Prism software (GraphPad Software Inc., La Jolla, CA, USA). A Tukey's posthoc test is performed.

Device design and rationale

Our design objective is to unite three beneficial attributes into a versatile, multiple-mode chamber array for cell culture and assay. The array is designed in a scalable, rectangular configuration so as to emulate the traditional well plate format with which life scientists are already familiar. In addition, other factors are considered in the design to provide additional experimental flexibility and reliability.

Three attributes

The first attribute is continuous perfusion. Continuous perfusion is desirable because it offers greater control of the cellular microenvironment when compared to traditional static culture. The concentration profile of any soluble signal of interest could be spatially and temporally controlled, whether the signal is pre-loaded into the medium or is secreted by cells in the chambers. Such control has proven useful in eliciting more physiological responses from a variety of cells in culture.[25–30]

The second attribute is the implementation of flow paths that forbid cross-chamber contamination. Flow paths are arranged such that once a streamline passes through a chamber, it does not pass through any other chambers before exiting the device. Therefore, there is no cross-talk from chamber to chamber, which eliminates the confounding effects of signals from neighboring chambers. This is especially important when cells are known to be highly-sensitive to signals present in other chambers (*i.e.* conditions) of the array or when the sensitivity of the cells to such signals is unknown. Additionally, fluid handling systems used with traditional well plate arrays are subjected to thorough cleaning procedures to minimize carryover contamination between wells.[31,32] For microfluidic arrays to yield biologically significant data, they must (among other things) meet or exceed the rigor of traditional systems in avoiding contamination.

The third attribute is a chamber design that reduces the shear stress applied to cells by shielding them from direct flow. One example of a shielded chamber is by Lee *et al.*,[8] where the majority of perfusing medium is diverted around a wall-like barrier, which surrounds a protected area where cells reside. Narrow conduits (gaps or mini-channels) in the barrier allow a small fraction of the overall flow to penetrate through the protected area and transport nutrients to the cells. The fraction of flow is determined by the hydraulic resistance of the conduits, which in turn is determined by their geometry. The chamber designed in this work is conceptually similar to the one just described. However, there is a notable difference: the chamber is designed so that flow enters and exits the protected area through conduits on the ceiling, a different plane from where the cells are attached. Flow must travel in three dimensions – vertically upward, horizontally across a conduit, then vertically downward. Two conduits serve as inlets at the upstream end of the chamber, and two serve as outlets at the downstream end (Fig. 1). The purpose is to avoid cell migration or proliferation into the conduits, which could block the flow path (see ESI Fig. 6). This is especially likely for cells that require seeding at high densities (*i.e.* epithelial cells).

Modes of operation

A key philosophy in designing the array is not only to combine the three attributes above, but also to provide considerable versatility to the user. Such versatility is demonstrated through multiple modes of operation and chamber addressing configurations. Fig. 2(b–e) show four basic modes of operation: (i) incubation of chamber surfaces with selected extracellular matrix (ECM) molecules; (ii) loading of cells into chambers; (iii) perfusion of selected growth media; and (iv) assay of cellular response to culture conditions. In addition to the addressing configurations illustrated in Fig. 2(b–e), other configurations can be implemented in order to generate more combinations of culture conditions or increase replicates. For instance, different

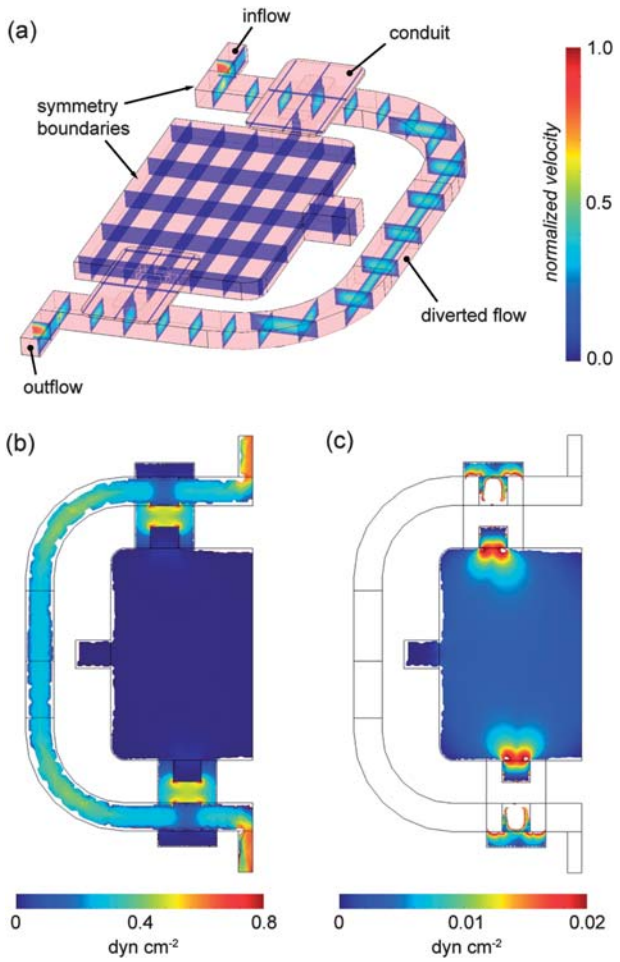

Fig. 4 Simulation of chamber flow field. (a) Oblique view of model geometry with solution shown in slice plot. Volumetric flow rate through diverted channel estimated as 90% of total flow (10% perfuses through protected area). (b) Shear stress field at floor of the chamber, solved using experimental flow rate. Shear on diverted surfaces is over an order of magnitude greater than in protected area. (c) Same solution as (b) with heat plot re-scaled to visualize shear stress in protected area; >85% of surface area less than 0.005 dyn cm^{-2}.

cell types could be loaded into separate rows, as opposed to a single cell type.

A compelling feature of the array is the ability to address individual chambers. Individual addressing is possible because four on-chip valves regulate flow into each chamber (two for column flow and two for row flow). When all four valves are closed, the chamber is fully isolated from the rest of the array. As a result, the experimentalist is given the opportunity to assign conditions or query a response with a high degree of specificity. If desired, different ECM molecules, cell types or assay reagents could be addressed to each chamber. As shown in Fig. 2(c), independent addressing is particularly useful during cell loading (see ESI Movie 1†). As the cell suspension flows across a row, the cell density tends to vary spatially, which is troublesome when the objective is to load each chamber with roughly the same number of cells. If the cell density in a chamber is unsuitable, then the valves can be opened momentarily and then closed again to sample a new set of cells. This can be repeated until the appropriate density is achieved. Furthermore, once a chamber is isolated, the flow of cells to other chambers continues uninterrupted, since cells can travel around isolated chambers *via* bypass channels. It is important to note that the ability to load cells by individual chambers also implies the ability to extract cells from an individual chamber of interest after the culture is completed.

Bridge-and-underpass architecture

Chambers in the device are arranged in a rectangular grid. This configuration is an obvious choice, since the chambers are efficiently packed in the grid, and it resembles rectangular arrays found in traditional well plates.

Less obvious is the architecture required to implement the rectangular array. In order to achieve the attributes and versatility described herein, it is necessary for flow streams to occasionally navigate over (or under) other flow streams as they travel through the array. This avoids cross flows. Flow streams navigate over (or under) other streams by traveling vertically between layers. Vertical flows take place within through-holes that fluidically link the layers. The result is a microfluidic channel network with three-dimensional flows that resemble roadway bridges and underpasses. Without the bridge-and-underpass architecture, the rectangular array configuration would be impossible.

The array device is comprised of three layers. The bottom layer contains flow channels, cell chambers, and control channels (for on-chip valve actuation). The middle layer contains through-holes that connect the top and bottom layers. The top layer contains flow channels, as well as conduits that allow flow into the protected areas of chambers (Fig. 1).

Results and discussion

In this work, we introduce a microfluidic living cell array, comprised of 8 culture chambers that do not cross-communicate, are continuously perfused, and are designed to protect cells from undesired shear stresses. This unique set of capabilities is demonstrated by studying the epithelial-to-mesenchymal transition (EMT) of alveolar epithelial cells in response to pairwise combinations of immobilized (Ln/Fn) and soluble (TGF-β1) signals. Because TGF-β1 induces the expression of numerous soluble factors, including additional TGF-β1,[33,34] cross-contamination among chambers in the array must be prevented for proper experimental control. Otherwise, cross-chamber contamination of soluble cues, including exogeneous or induced TGF-β1 secretion, would produce confounding phenotypes. The features introduced herein make it possible for well-controlled interrogation with different signal combinations under ideal culture conditions in a versatile and scalable chamber array

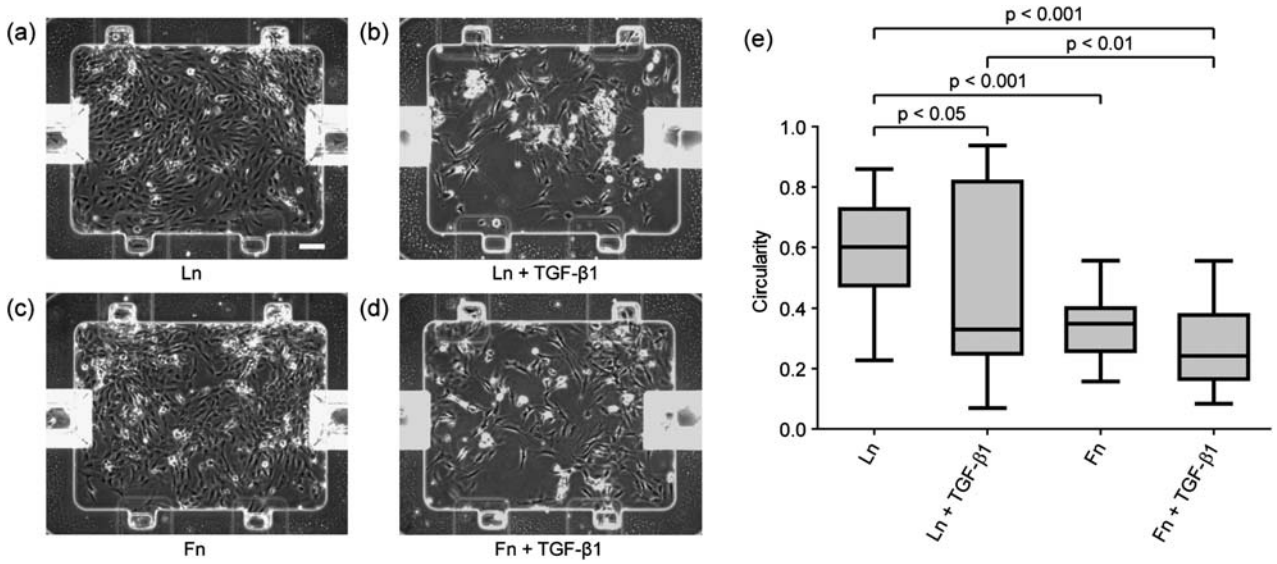

Fig. 5 Phase contrast images (representative) of ATII cells after 2 d culture. Matrix and soluble factor signaling combinations of (a) Ln, (b) Ln + TGF-β1, (c) Fn, (d) Fn + TGF-β1. Monolayer with extensive cell–cell contacts suggests epithelial phenotype in Ln condition. Lower relative density suggests decreased proliferation and/or apoptotic events for Ln + TGF-β1 condition. (e) Box plot of cell circularity for each signal combination. Calculated from traces of 30 randomly selected cells (3 trials, 10 per trial) for each signal combination. Boxes span 25th to 75th quartiles (median line inside) with lower and upper extreme values noted by whiskers. Significant p-values in brackets. Scale bar 100 μm.

format. Multiplexing with the array makes it easy to load cells and reagents with minimum dead volume in the system, hence saving reagents.

Device characterization

We have successfully fabricated the array device using the adapted through-hole process described earlier. We found that yield is significantly improved if we apply the following modifications. When weight is applied, the pressure is focused above each device by adding small transparency sheets cut to the size of devices on top of the transparency stack (ESI Fig. 1). We observed that this improves through-hole yield, presumably because it assists in displacing PDMS from the tops of SU-8 features by providing a nearby reservoir between devices into which PDMS can flow. We also use soft cloths (Texwipes) in the stack, further improving the through-hole yield by providing a more uniform distribution of pressure across the master and over each device. In addition, the PDMS is partially cured (in lieu of fully cured) so it can be thermally bonded to a subsequent PDMS layer (from master B). The thermal bonding technique provides ample time to properly align the two PDMS layers. This differs with air plasma bonding, which affords far less time (<1 min after plasma surface activation). Extra time is beneficial, particularly for manual alignments, or for aligning multiple devices on a single master, which could take more than a minute to complete (whether manual or automated).

An array device loaded with colored dyes (water as carrier fluid) is shown in Fig. 3. Individual addressing offers the versatility to load different cells or adsorb different matrix molecules in each chamber (Fig. 3(b–c)). Also, individual addressing allows the experimentalist to fine-tune the cell density in each chamber by momentarily re-opening and closing chamber isolation valves to sample different sets of cells as they flow into the device; this process was essential to achieving uniform cell densities across chambers for the experiments performed in this work (see ESI Movie 1). Fig. 3(d–f) shows how flow travels through the chamber. Flow enters from a common delivery channel and is expelled into a common exit channel that does not feed into other chambers. Careful inspection of Fig. 2 and 3 reveals that a 3-dimensional flow network is vital to prevent cross-chamber contamination in an array that is continuously-perfused and has a rectangular configuration. We use the strategies demonstrated in Fig. 3 to adsorb different ECM molecules as well as perfuse TGF-β1-containing medium to different chambers for the experiments summarized in Fig. 5–7.

Fig. 4 shows results of the chamber flow field simulation. Integration of velocities at selected boundaries shows that approximately 10% of the total flow through the chamber travels through the protected area (1 : 10, protected-to-total flow ratio). The balance of flow travels through the diverted flow channels. In addition, shear stresses are calculated on the surface of the chamber at experimental flow rates. Too much flow can result in high velocity and high shear, which may be detrimental to the cells; on the other hand, not enough flow will reduce the availability of nutrient and gas exchange, which may also affect cells adversely. Having the shielded chamber design allows ample amount of convective mass transfer and yet avoids direct shear on the cells inside the chamber. We show here that the shear inside the chamber is negligible.

Because the array was designed as a prototype to demonstrate initial proof-of-concept, the array is small relative to other arrays reported in the literature. Scaling the array to larger sizes will require more control channels (and corresponding outlet ports) for the additional chambers. Additional challenges include the increased complexity of the device; however, others[18,35] have shown that such additional complexity is manageable.

ATII response to soluble-matrix signal combinations

We use the array to study phenotypes expressed by ATII cells when subjected to four different soluble-matrix signal combinations, particularly ones that have been demonstrated to lead to three different cellular responses; specifically, maintenance of

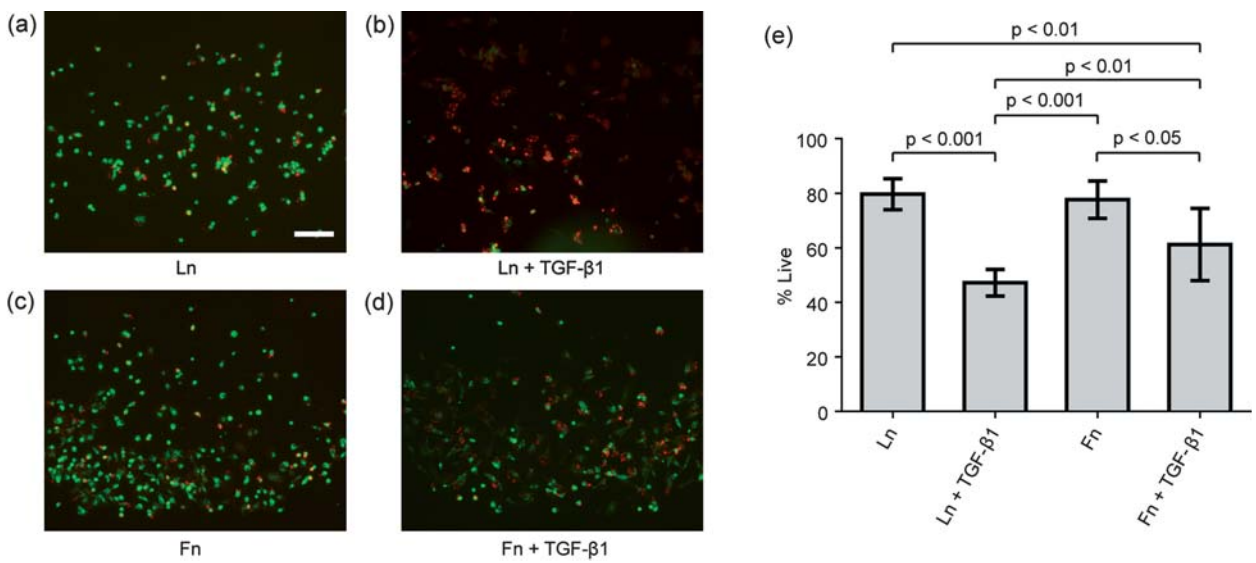

Fig. 6 Viability of ATII cells after 2 d culture assessed by LIVE/DEAD fluorescent staining. Representative fluorescence images (green/red composite overlays) showing entire chamber for each matrix and soluble factor signaling combination: (a) Ln, (b) Ln + TGF-β1, (c) Fn, (d) Fn + TGF-β1. (e) Percentage of live (green) cells for each condition (6 trials each); error bars show SD. Significant p-values in brackets. Scale bar 100 μm.

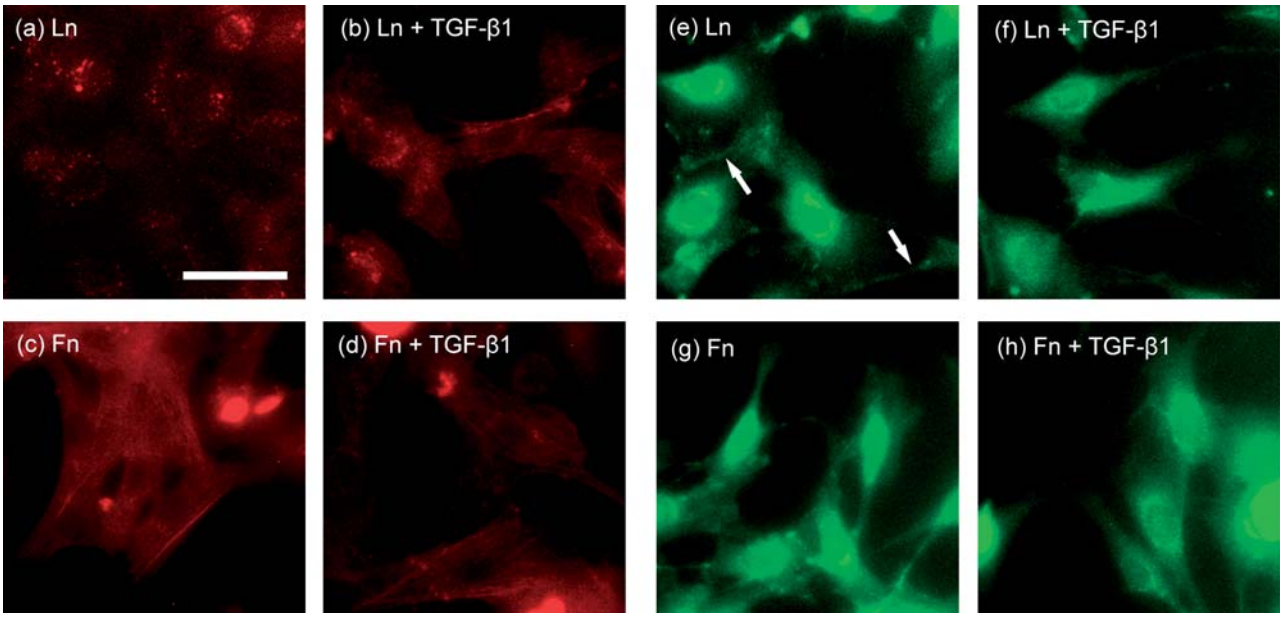

Fig. 7 Cytoskeletal organization and cell–cell junction formation of ATII cells after 2 d culture. False color fluorescent images of actin stress fibers stained with Texas Red-phalloidin for each matrix and soluble signaling combination: (a) Ln, (b) Ln + TGF-β1, (c) Fn, and (d) Fn + TGF-β1. Stress fiber formation prominent in Fn conditions (with and without TGF-β1). Stress fibers also observed in Ln + TGF-β1 condition. Ln condition shows diffuse staining. False color images of immunofluorescently-labeled E-cadherin shown in (e)–(h). Arrows in (e) indicate localization of E-cadherin at cell–cell contacts and cell edges. Scale bar 50 μm.

epithelial phenotype, cellular apoptosis, and epithelial-to-mesenchymal transition (EMT). EMT is a process where fully differentiated epithelial cells undergo a transition to a mesenchymal phenotype, resulting in fibroblasts and myofibroblasts. EMT can be induced by a number of extracellular signals,[33] individually or in combination, and EMT is known to play a role in development and tumor invasion.[36–38] In addition, EMT is observed in response to epithelial stress or injury in a variety of tissues, where it is involved in repair and scar formation.[39–41] EMT in the context of epithelial injury and fibrosis is not well understood, and recent literature is just beginning to address its underlying mechanisms.[42]

EMT of ATII cells has been implicated in idiopathic pulmonary fibrosis (IPF).[42] IPF is a fatal condition characterized by excessive ECM deposition, resulting in interstitial scar tissue, loss of tissue compliance and ultimately decreased gas exchange across the alveolar epithelial barrier. Under normal conditions, ATII cells perform multiple roles in the lung associated with proper homeostasis and repair; in response to injury to the alveoli, ATII cells proliferate and differentiate into ATI cells. However, in fibrosis, ATII cells appear to undergo EMT, driving the cells toward a fibroblastic (mesenchymal) phenotype. This increases the number of ECM-depositing mesenchymal cells in the interstitial space and further perpetuates the fibrotic condition.

Elevated levels of active TGF-β1 and deposition of a provisional matrix rich in Fn are prominent components of pulmonary fibrosis, whereas a matrix rich in Ln is typical of homeostatic physiological conditions. Previous studies have demonstrated that ATII cells undergo markedly different behavioral responses to TGF-β1 depending on their underlying substrate.[42] In the presence of TGF-β1, ATII cells adhering to Ln-rich matrices undergo apoptosis, whereas on Fn-rich matrices they exhibit EMT-like events. To query and confirm the response of ATII cells to the aforementioned signals, array chambers were incubated with Fn or Ln and perfused with medium with and without active TGF-β1. All signal combinations were present in each array and repeated by subarray.

Cell morphologies in response to each signal combination after 48 h in culture are shown in Fig. 5. Cells cultured on Ln in the presence of TGF-β1 show either contracted morphology (indicative of cell death) or elongated morphology. Cells cultured on Fn in the presence of TGF-β1 show similar elongation, resembling a fibroblastic phenotype and indicating induction of alveolar EMT in the presence of the potent TGF-β1 cytokine. For cells cultured on Fn in the absence of TGF-β1, a similar fibroblastic morphology results. This is consistent with reports showing that Fn is capable of driving differing phenotypes for multiple cell types and inducing EMT in alveolar cells.[42–45] Cells cultured on Ln in the absence of TGF-β1 show a round, semi-cuboidal morphology and are arranged in an orderly monolayer. This suggests that ATII cells cultured on Ln (no TGF-β1) follow the "normal" ATII differentiation pathway and retain an epithelial phenotype on-chip, consistent with culture using conventional methods in cell culture dishes. When cultured on Ln in the presence of TGF-β1, the lower density of cells, as well as the prevalence of contracted morphologies, suggests a phenotype that is prone to apoptosis, which has been recently reported.[42] Circularity is calculated for cells in each signal combination, showing quantifiable differences in morphologies (Fig. 5(e)). In the Ln with TGF-β1 condition, cells with contracted, round morphologies (appearing to go into apoptosis) exist with highly-elongated cells (fibroblastic), causing the relatively wide variation in data for that condition. Cell areas are plotted in ESI Fig. 5. The absence of statistically significant

differences indicates that cell shape, rather than cell size, is more affected by the conditions.

To quantify cell viability for each combination of soluble and matrix cues, cells are stained with LIVE/DEAD fluorescent probes (Fig. 6). Without TGF-β1, cells are predominantly viable. For conditions perfusing TGF-β1, larger fractions of cells are shown to be dead (red stain, Fig. 6(b) and (d)). The lowest viability is measured for cells on Ln in the presence of TGF-β1, which agrees with the morphological observations and the previously mentioned report.[42]

To further characterize the morphological differences observed for each signal combination, we analyze cytoskeletal organization and stress fiber formation in cells by staining F-actin with Texas Red phalloidin (Fig. 7(a-d)). Stress fiber formation, a direct indicator of cell contractility and indirect indicator of mesenchymal-like phenotypes, is evident in the three combinations with Fn and/or TGF-β1 (Fig. 7(b–d)). The diffuse staining observed in cells on Ln (no TGF-β1) is typical of epithelial cells, suggesting a more normal physiological phenotype.

EMT is also characterized by the disassembly of epithelial cell–cell junctions. Junctions are marked by cell–cell adhesion proteins (*e.g.* E-cadherin) concentrated at cell edges. To visualize E-cadherin, cells are immunofluorescently-labeled and imaged at each condition (Fig. 7(e–h)). Labeling of E-cadherin in the three combinations with Fn and/or TGF-β1 (Fig. 7(f–h)) appears diffuse with perinuclear localization. This suggests a loss of normal epithelial characteristics,[46,47] which could be the result of a presumably EMT-like shift toward a more fibroblastic phenotype. Concentration of E-cadherin at cell–cell contacts in the Ln (no TGF-β1) condition further suggests retention of an epithelial phenotype (Fig. 7(e)).

Taken together, the biological data suggest that cells assume a mesenchymal phenotype when cultured in signal combinations that include Fn or TGF-β1, while cells cultured on Ln (no TGF-β1) retain an epithelial phenotype. In addition, Ln with TGF-β1 leads to an apoptosis-prone phenotype. These results are consistent with prior findings.

The study herein validates the array as a unique platform to culture cells under combinations of signals. The results suggest that the microfluidic array chip can provide equivalent long-term culture conditions suitable to study combinatorial treatments of cells, and that the phenotypes of cells are preserved in such conditions as compared to conventional culture and imaging. Furthermore, the microfluidic chip allows for replicates and controls to be performed on the same chip at the same time. The array architecture is particularly well-suited to present soluble-matrix signal combinations in order to elicit and distinguish phenotype transitions. Moreover, the device can be extended to other cell types and transitional phenomena, in addition to EMT.

Conclusions

In this work, we designed, built, and validated a microfluidic chamber array that can present cells with different signaling combinations comprised of both soluble and matrix factors. To provide a unique set of capabilities desirable to life scientists, the array operates with continuous perfusion, prevents cross-chamber contamination, protects cells from excessive shear, and offers considerable experimental versatility. These attributes are made possible by implementing a 3-dimensional flow network (bridge-and-underpass architecture), which is fabricated using a modified compression-molding technique.

By characterizing the extent of EMT in ATII cells, we validate the array as a screening tool, particularly for studying phenotype transitions and cellular behavior under combinatorial soluble and matrix conditions. The expression of these phenotypes is particularly sensitive to the extracellular environment, which highlights the utility of the non-cross-contaminating chamber array shown in this work. Given that cellular response mechanisms are tremendously complex, this array technology is ideal to perform studies where cellular response is very sensitive to microenvironmental conditions within a parallelized, well-controlled, efficient microfluidic format.[48] Furthermore, the array could be used to perform studies under different perfusion rates (in combination with soluble and matrix signals) or adapted to stimulate cells with time-varying signal patterns. By further scaling up the array and implementing greater automation, such a setup will lead to higher control and throughput, making the array capable of more sophisticated studies. These studies could lead to insights into the mechanisms for the onset and progression of pathological phenotype transitions, like EMT, and the identification of novel therapeutic targets to treat diseases.

Acknowledgements

The authors thank Kwanghun Chung for helpful discussions, Jeffrey N. Stirman and Matthew M. Crane for assistance with computer automation, and Mei Zhan for assistance with 3D figures. EP was supported by a National Defense Science and Engineering Fellowship, and HL is a DuPont Young Professor and a Sloan Research Fellow.

Notes and references

1 Y. Soen, A. Mori, T. D. Palmer and P. O. Brown, *Mol. Syst. Biol.*, 2006, **2**, art. 37.
2 J. H. Jang and D. V. Schaffer, *Mol. Syst. Biol.*, 2006, **2**, art 39.
3 C. J. Flaim, D. Teng, S. Chien and S. N. Bhatia, *Stem Cells Dev.*, 2008, **17**, 29–39.
4 T. G. Fernandes, M. M. Diogo, D. S. Clark, J. S. Dordick and J. M. S. Cabral, *Trends Biotechnol.*, 2009, **27**, 342–349.
5 J. El-Ali, P. K. Sorger and K. F. Jensen, *Nature*, 2006, **442**, 403–411.
6 B. Angres, *Expert Rev. Mol. Diagn.*, 2005, **5**, 769–779.
7 C. J. Wang, X. Li, B. Lin, S. Shim, G. L. Ming and A. Levchenko, *Lab Chip*, 2008, **8**, 227–237.
8 P. J. Lee, P. J. Hung, V. M. Rao and L. P. Lee, *Biotechnol. Bioeng.*, 2006, **94**, 5–14.
9 P. J. Hung, P. J. Lee, P. Sabounchi, R. Lin and L. P. Lee, *Biotechnol. Bioeng.*, 2005, **89**, 1–8.
10 P. J. Hung, P. J. Lee, P. Sabounchi, N. Aghdam, R. Lin and L. P. Lee, *Lab Chip*, 2005, **5**, 44–48.
11 D. Di Carlo, L. Y. Wu and L. P. Lee, *Lab Chip*, 2006, **6**, 1445–1449.
12 Z. H. Wang, M. C. Kim, M. Marquez and T. Thorsen, *Lab Chip*, 2007, **7**, 740–745.
13 D. M. Thompson, K. R. King, K. J. Wieder, M. Toner, M. L. Yarmush and A. Jayaraman, *Anal. Chem.*, 2004, **76**, 4098–4103.
14 S. Sugiura, J. Edahiro, K. Kikuchi, K. Sumaru and T. Kanamori, *Biotechnol. Bioeng.*, 2008, **100**, 1156–1165.
15 K. R. King, S. H. Wang, D. Irimia, A. Jayaraman, M. Toner and M. L. Yarmush, *Lab Chip*, 2007, **7**, 77–85.
16 A. Khademhosseini, J. Yeh, G. Eng, J. Karp, H. Kaji, J. Borenstein, O. C. Farokhzad and R. Langer, *Lab Chip*, 2005, **5**, 1380–1386.
17 H. Y. Wang, N. Bao and C. Lu, *Biosens. Bioelectron.*, 2008, **24**, 613–617.
18 R. Gomez-Sjoberg, A. A. Leyrat, D. M. Pirone, C. S. Chen and S. R. Quake, *Anal. Chem.*, 2007, **79**, 8557–8563.

19 L. Kim, Y. C. Toh, J. Voldman and H. Yu, *Lab Chip*, 2007, **7**, 681–694.
20 J. C. McDonald, D. C. Duffy, J. R. Anderson, D. T. Chiu, H. K. Wu, O. J. A. Schueller and G. M. Whitesides, *Electrophoresis*, 2000, **21**, 27–40.
21 M. A. Unger, H. P. Chou, T. Thorsen, A. Scherer and S. R. Quake, *Science*, 2000, **288**, 113–116.
22 M. J. Madou, *Fundamentals of microfabrication: the science of miniaturization*, CRC Press, Boca Raton, 2002.
23 A. Folch, B. H. Jo, O. Hurtado, D. J. Beebe and M. Toner, *J. Biomed. Mater. Res.*, 2000, **52**, 346–353.
24 L. Kim, M. D. Vahey, H. Y. Lee and J. Voldman, *Lab Chip*, 2006, **6**, 394–406.
25 R. M. Schwartz, B. O. Palsson and S. G. Emerson, *Proc. Natl. Acad. Sci. U. S. A.*, 1991, **88**, 6760–6764.
26 W. W. Minuth, P. Steiner, R. Strehl, K. Schumacher, U. de Vries and S. Kloth, *Experimental Nephrology*, 1999, **7**, 394–406.
27 W. W. Minuth, J. Aigner, S. Kloth, P. Steiner, M. Tauc and M. L. Jennings, *Pediatr. Nephrol.*, 1997, **11**, 140–147.
28 E. Leclerc, B. David, L. Griscom, B. Lepioufle, T. Fujii, P. Layrolle and C. Legallaisa, *Biomaterials*, 2006, **27**, 586–595.
29 K. Blagovic, L. Kim, A. M. Skelley and J. Voldman, in *Twelfth International Conference on Miniaturized Systems for Chemistry and Life Sciences*, San Diego, California, USA, 2008, pp. 677–679.
30 L. Aubry, J. Tournois, M. Girard, A. L. Perrier, M. Peschanski, M. Cailleret, J. Come and X. Nissan, *Tissue Engineering Part C Methods*, 2008, **14**, 289–298.
31 M. G. O. Lorenz, *J. Assoc. Lab. Autom.*, 2004, **9**, 262–267.
32 C. J. Frégeau, C. Yensen, J. Elliott and R. M. Fourney, *J. Assoc. Lab. Autom.*, 2007, **12**, 339–354.
33 J. Zavadil and E. P. Bottinger, *Oncogene*, 2005, **24**, 5764–5774.
34 R. Derynck, R. J. Akhurst and A. Balmain, *Nat. Genet.*, 2001, **29**, 117–129.
35 http://www.fluidigm.com/.
36 J. P. Thiery, *Nat. Rev. Cancer*, 2002, **2**, 442–454.
37 A. Nawshad, D. LaGamba, A. Polad and E. D. Hay, *Cells Tissues Organs*, 2005, **179**, 11–23.
38 G. Greenburg and E. D. Hay, *J. Cell Biol.*, 1982, **95**, 333–339.
39 S. Saika, S. Kono-Saika, Y. Ohnishi, M. Sato, Y. Muragaki, A. Ooshima, K. C. Flanders, J. Yoo, M. Anzano, C. Y. Liu, W. W. Y. Kao and A. B. Roberts, *Am. J. Pathol.*, 2004, **164**, 651–663.
40 Y. H. Liu, *J. Am. Soc. Nephrol.*, 2004, **15**, 1–12.
41 R. Kalluri and E. G. Neilson, *J. Clin. Investigation*, 2003, **112**, 1776–1784.
42 K. K. Kim, M. C. Kugler, P. J. Wolters, L. Robillard, M. G. Galvez, A. N. Brumwell, D. Sheppard and H. A. Chapman, *Proc. Natl. Acad. Sci. U. S. A.*, 2006, **103**, 13180–13185.
43 D. Sheppard, *BioEssays*, 1996, **18**, 655–660.
44 G. Serini and G. Gabbiani, *Exp. Cell Res.*, 1999, **250**, 273–283.
45 J. L. Jones and R. A. Walker, *Mol. Pathol.*, 1999, **52**, 208–213.
46 G. Handschuh, S. Candidus, B. Luber, U. Reich, C. Schott, S. Oswald, H. Becke, P. Hutzler, W. Birchmeier, H. Hofler and K. F. Becker, *Oncogene*, 1999, **18**, 4301–4312.
47 F. Balzac, M. Avolio, S. Degani, I. Kaverina, M. Torti, L. Silengo, J. V. Small and S. F. Retta, *J. Cell Sci.*, 2005, **118**, 4765–4783.
48 M. L. Yarmush and K. R. King, *Annu. Rev. Biomed. Eng.*, 2009, **11**, 235–257.

